Noise-driven switching between limit cycles and adaptability in a small-dimensional excitable network with balanced coupling

Leonid A. Safonov* and Yoshiharu Yamamoto†
Educational Physiology Laboratory, Graduate School of Education, The University of Tokyo, 7-3-1 Hongo, Bunkyo-ku, Tokyo 113-0033, Japan
(Received 13 June 2005; revised manuscript received 3 January 2006; published 15 March 2006)

We study a system of globally coupled FitzHugh-Nagumo equations. Each unit is either excitatory or inhibitory. If the numbers of units of both types are in a specific ratio, we observe the presence of multistable oscillatory states with different excitation or *firing* rates. In the presence of noise, there is noise-driven switching between these states and the resultant firing pattern is long-range correlated. The choice between higher and lower frequency oscillations depends on the input, which results in increasing adaptability of the system's output to the periodic input.

DOI: 10.1103/PhysRevE.73.031914 PACS number(s): 87.10.+e, 84.35.+i, 05.45.−a

I. INTRODUCTION

Stable biological oscillators are usually modeled by limit cycles [1,2]. Limit cycles show *stability* in their "activity," when evaluated by both the amplitude and frequency, over a wide range of control parameters, including external force. For example, in neural models such as FitzHugh-Nagumo (FHN) [3] and Hodgkin-Huxley [4] equations, the activity does not change much when they are forced by inputs above their "firing" threshold.

In contrast, networking limit cycles [1,5] or general nonlinear elements [6] are known to produce diverse spatiotemporal (synchronized) patterns with different frequencies and amplitudes, giving rise to variable activity levels over the whole network. Each pattern corresponds (in a broad sense) to a stable attractor, and the existence of multistable attractors with different activity levels may account for *diversity* or *variability* in real-world oscillators, including biological ones.

Here we consider the *adaptability* issue, which is one of the unique characteristics of living organisms. Such a characteristic is widely observed: a network of neurons or neural assemblies showing limit cycle type behavior, like the brain, changes its dynamics by sensory inputs. A population of biological organisms, modeled by coupled oscillators [1,7] may need to change its activity depending on the physical and/or chemical surroundings. The question to ask is whether the selection of multistable attractors in coupled oscillators depends on the level of external forcing, meaning that the network activity is coherent with the forcing. To our knowledge, this rather intuitive problem has never been studied in an explicit manner.

In the present paper, we study a system of globally coupled suprathreshold FHN equations with external forcing and noise. Each unit is either excitatory or inhibitory. If the numbers of units of both types are in a specific ratio (balanced coupling), we observe the presence of multistable oscillatory states with different excitation (firing) rates, and switches between high- and low-frequency oscillatory states can occur easily in the presence of noise. In the presence of an optimal level of noise, in particular, the system demonstrates considerably improved coherence between the external forcing and the mean firing rate, similar to what is known as the stochastic resonance (SR) [8,10] and coherence resonance [9], indicating that the selection of multistable attractors with different activity levels is statistically more "ordered" in response to the changes in the external forcing. We conclude that the coexistence of inhibitory and excitatory connections and the noise effect is a key to observing higher *adaptability* in this network of nonlinear oscillators.

II. THREE GLOBALLY COUPLED FITZHUGH-NAGUMO EQUATIONS

We consider a system of coupled units whose dynamics is described by the FHN equations,

$$\varepsilon \dot{v}_i = v_i(v_i - a)(1 - v_i) - w_i + I + S(t) + \frac{1}{N}\sum_{j=1}^{N} k_{ij}(v_j - v_i) + \xi_i(t),$$

$$\dot{w}_i = v_i - w_i - b, \tag{1}$$

where $\varepsilon = 0.005$, $a = 0.5$, $b = 0.15$, I is a constant input, $S(t)$ is a time-dependent input, $i, j = 1, \ldots, N$, $\xi_i(t)$ is Gaussian white noise with $\langle \xi_i(t)\xi_j(s)\rangle = 2D\delta_{ij}\delta(t-s)$, where $\langle \cdots \rangle$ denotes the ensemble average, and $2D \cdot \Delta t = \langle \xi_i^2(t)\rangle = \sigma^2$ in the discrete case. We assume that each unit provides only one type of connection (excitatory or inhibitory) to other units, and is therefore referred to as either excitatory or inhibitory. If the jth unit is excitatory then $k_{ij} > 0$ and if it is inhibitory $k_{ij} < 0$. Computations are performed using the stochastic second order Runge-Kutta algorithm [11] with the time step of 0.002.

For a single uncoupled unit, there is a stable stationary solution for small I. At $I_0 \approx 0.11$ a Hopf bifurcation produces a stable limit cycle, which corresponds to the excited (or *firing*) state of the unit.

*Electronic address: safonov@p.u-tokyo.ac.jp
†Electronic address: yamamoto@p.u-tokyo.ac.jp

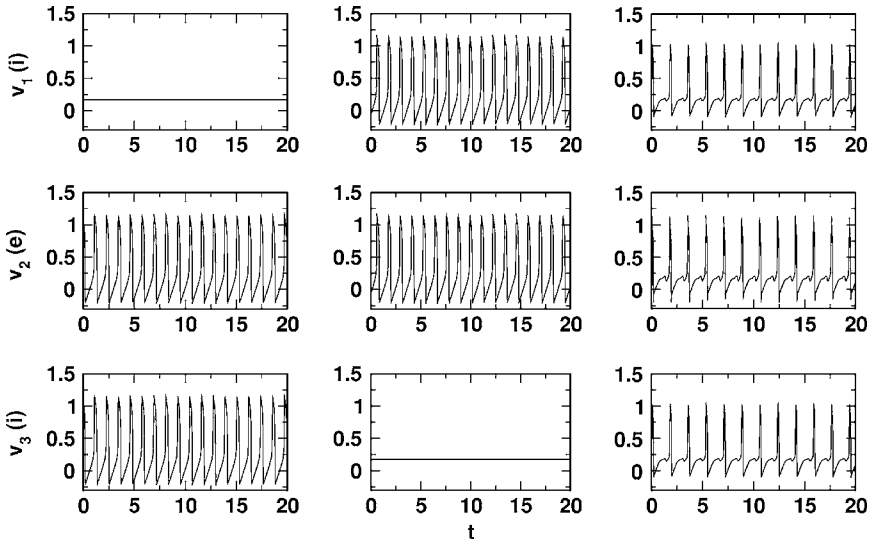

FIG. 1. Firing regimes for attractors 1 (left-hand side), 2 (center), and 3 (right-hand side). $N=3$, $N_E=1$, $I=0.07$. The second unit is excitatory (**e**), the others are inhibitory (**i**).

The adaptability of excitation or *firing* rates in the suprathreshold regime to changing levels of I can best be understood by studying the system's dynamics for $N=3$ with four possible choices of the number of excitatory units (N_E).

A. $N_E=1$

First, we study the case of three units, one of which is excitatory and the other two are inhibitory, without noise. The coupling strength of each connection is taken to be equal to $|k|=0.3$ with a corresponding sign.

At $I_1 \approx 0.057$ there is a double resonant Hopf bifurcation, at which two stable limit cycles emerge. They have two firing units and one silent, and are located in the following invariant subspaces:

$$x_1 = C, \quad x_2 = x_3; \tag{2}$$

$$x_3 = C, \quad x_1 = x_2, \tag{3}$$

where $x_i=(v_i,w_i)$ and C is a constant value ("resting potential"). The plots of v variables of these cycles are shown in Fig. 1 (left-hand and central columns).

Along with the two cycles, there is a third stable attracting set (with all three units firing) emerging at or near the double Hopf bifurcation and located in the invariant subspace,

$$x_1 = x_3. \tag{4}$$

With a growing parameter I, it has the form of a limit cycle for most of the parameter values. A typical firing pattern for this cycle is shown in Fig. 1 (right-hand column). Figure 2 shows the dependence on I of the two Floquet multipliers of this limit cycle with the largest absolute value [12]. At certain parameter values, this cycle undergoes bifurcations transforming it into a higher-periodic attracting set (possibly nonperiodic for some parameter values) with the period dependent on the parameter. Figure 3 gives examples of firing patterns of this attractor for I values for which it is not a simple limit cycle.

In the following, we refer to these three attractors as attractors 1, 2, and 3, respectively. Attractors 1, 2 are also referred to as limit cycles 1, 2, because they do not take any other form.

Multistability in coupled FHN equations has been studied in Ref. [13], and in a single FHN equation with periodic forcing in Ref. [14]. The former paper deals with two units with mutually inhibitory coupling, and it is known that inhibition is important for producing multistability in neuronal models [15].

With increasing I, we observe that the firing rate (number of spikes per time unit) R of cycles 1 and 2 grows rapidly over a short parameter interval, after which it changes only insignificantly (Fig. 4). In contrast, the firing rate of attractor 3 grows slowly with I for a long interval, after which it stabilizes.

At $I_0 \approx 0.11$ (as in the single unit case) there is an ordinary Hopf bifurcation, where the stationary solution becomes globally unstable and a new limit cycle emerges. In the present study we consider values of I between I_1 and I_0, where the firing rates of all the attractors are relatively stable (shown by shaded areas in Figs. 2, 4, 13, and 14). In this regime, no stable attractor solely has a sufficient rate coding ability for the external input I; see flat curves in Fig. 2.

From numerical simulations, we find that the domain of attraction of the stationary solution coincides with the subspace

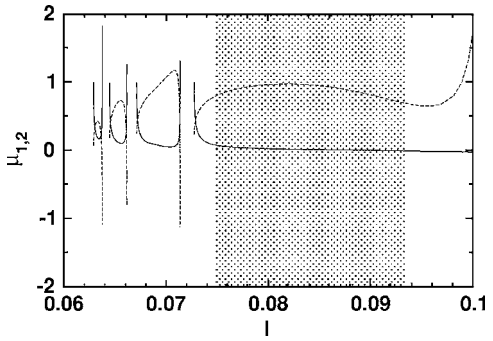

FIG. 2. Two Floquet multipliers with the largest absolute value of attractor 3 for I values for which it is a simple limit cycle.

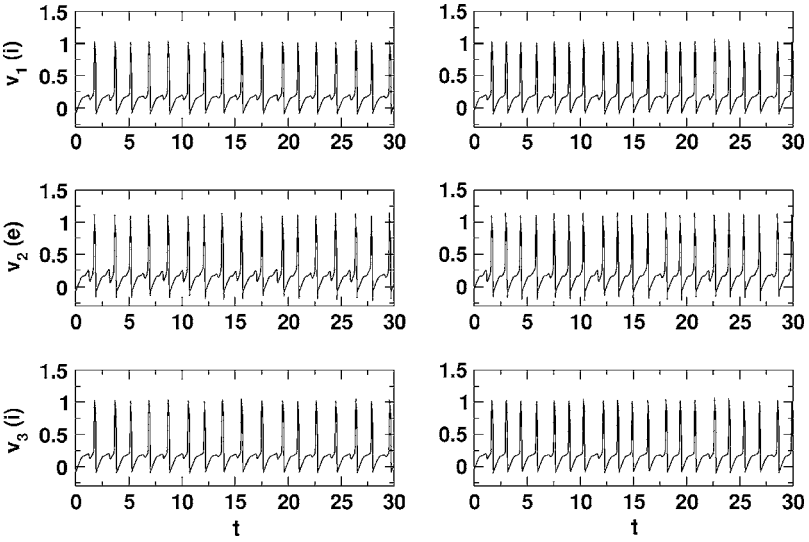

FIG. 3. Firing patterns of attractor 3 for $I=0.0715$ (left-hand side) and $I=0.0725$ (right-hand side).

$$x_1 = x_2 = x_3, \tag{5}$$

the domain of attraction of attractor 3 is located around the subspace (4) except subspace (5), while cycles 1 and 2 attract trajectories originating from the rest of the phase space.

In the presence of weak noise, the system performs random transitions between domains of attraction of the three attractors (Fig. 5). This is similar to a phenomenon known as chaotic itinerancy (CI) [6]. CI has been observed in various natural systems and evidence of it has been found in neural ensembles [16,17]. It has also been demonstrated by neuronal models [18–22]. CI is characterized by successive visits by an orbit to vicinities of low-dimensional structures ("attractor ruins"). These structures have different synchronization properties, and escape from an attractor ruin follows a restricted path, which makes the dynamics different from random hopping among attractors. The difference with our system is that instead of chaotic attractors, we have limit cycles, and the role of noise is to induce itinerant dynamics. In addition to chaotic itinerancy other types of complex behavior in neural systems related to transitions between attractors have been studied, such as winnerless competition [23].

It has been suggested in Ref. [6] that hopping between attractor ruins in CI is not random but adheres to certain constraints. In our case, transitions between cycles 1 and 2 do not occur, and the only transitions possible are $1 \leftrightarrow 3 \leftrightarrow 2$. This is related to the fact that cycles 1 and 2 lie in such invariant subspaces [(2) and (3)] that in order for a transition between them to occur, an orbit must come close to the subspace (4), which belongs to the domain of attraction of attractor 3. Such alternations between fully and partly synchronized dynamics have been observed in globally coupled chaotic maps [6].

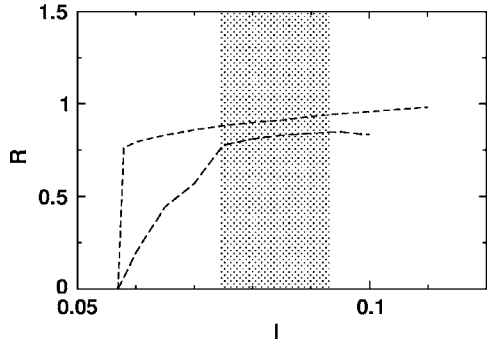

FIG. 4. Dependence of the firing rate on the input I for $N=3$ and $N_E=1$. Upper line, high-frequency regimes (cycles 1 and 2); lower line, low-frequency regime (attractor 3).

One of the characteristic features of CI is power-law correlations. It has been conjectured in Ref. [24] that a multistable system with noise-induced jumps between attractors exhibits $1/f^{\alpha}$ power spectrum at low frequencies with $\alpha \sim 0.5-1.5$. Similar phenomena have been found in an iterative map [25] and in a semiconductor laser model [26]. Power-law temporal and spatial correlations are also one of the characteristic features of brain dynamics [16].

Similarly, in our study we observe the presence of $1/f$ dynamics for small noise (e.g., $\sigma^2=2\times10^{-9}$). Figure 6 presents power spectra of instantaneous firing rates (IFR [27]) of excitatory and inhibitory units with $I=0.09$. It can be seen that spectral properties of excitatory and inhibitory units are different.

This difference is related to the different firing patterns of these types of units (Fig. 5, left-hand side). As was argued in Ref. [6], the emergence of long-range correlations in chaotic itinerancy results from the fact that the itinerancy between attractors is not random, but follows a certain restricted path. Due to this the system retains memory about previously visited attractor ruins, and the resulting orbits are history dependent. In the system under consideration, an inhibitory unit iterates between three firing patterns, while an excitatory unit has a choice of only two. Since the visits to cycle 3 are very brief compared to visits to cycles 1 and 2 (except for very small noise), an inhibitory unit essentially iterates between silent and fast-firing patterns, only briefly passing to the slow-firing one, and the memory is generated only regarding the former two states. On the contrary, an excitatory unit stays almost exclusively in the fast-firing pattern, occasionally and briefly jumping to the slow-firing one, so that the long-term memory is not created, and long-range correlations are absent.

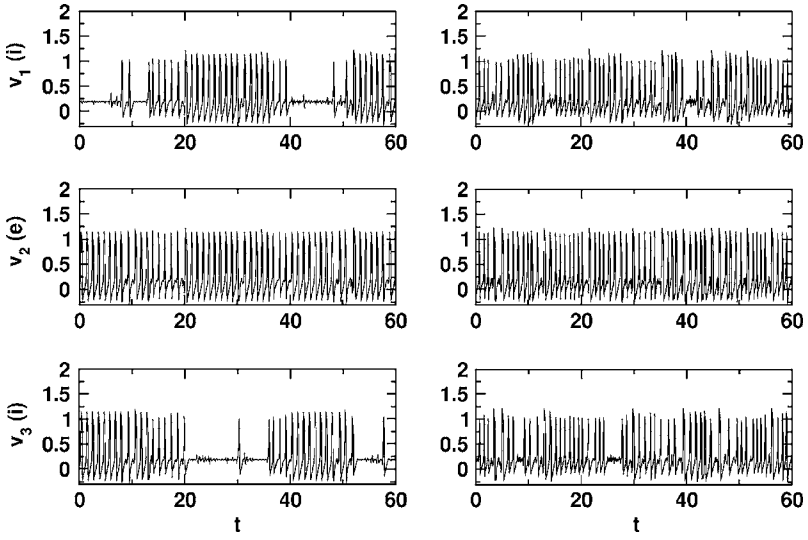

FIG. 5. Itinerant oscillations in the presence of noise. $N=3$, $N_E=1$, $I=0.09$, $\sigma^2=10^{-7}$ (left-hand side), 10^{-5} (right-hand side). With strong noise random firing dominates over limit cycle oscillations (right-hand side).

The system also demonstrates phenomenon similar to SR in rate coding. We apply periodic input $S(t)$ to all units and plot the coherence measure

$$C_0 = \overline{S(t)R(t)},$$

[where $R(t)$ is the IFR and the overbar denotes the time average] against the noise intensity. As in the case of correlations, excitatory and inhibitory neurons have different properties.

Figure 7 shows the dependence of C_0 on the noise intensity for different baseline input and amplitude of periodic input. We can observe the bell-shaped curve, especially for IFR of excitatory units, characteristic of SR. This phenomenon resembles suprathreshold stochastic resonance studied previously [28], but has a different dynamical nature, as explained below.

Figures 8(a)–8(d) show sample spike trains of an excitatory and an inhibitory unit for weak and moderate noise intensities, respectively. Although for most of the time the system stays near attractors 1 or 2, occasionally it jumps to attractor 3, and the probability of such a transition is higher for lower input than for higher input.

Limit cycle oscillations on all attractors consist of spike (action potential) time and silent (resting potential) time. With the increase of firing rate, the spike time remains almost the same, while the resting time decreases. Transitions between the attractors are most likely during the resting time when the distance to other attractors is minimal. Since this time is longer for lower input, a switch to another attractor is more likely to happen with a lower input. The average duration of a visit to attractor 3 is small compared to that of other attractors, therefore a transition to attractor 3 near the minimal input is followed by a switch to another attractor while the input is still close to the minimum.

With stronger noise the transition probability becomes higher, and the time spent by the orbit near attractor 3 is greater. Therefore the resulting IFR of an excitatory unit is more coherent with the input for moderate noise [Fig. 8(d)] than for weak noise [Fig. 8(b)]. Thus, an increase of noise

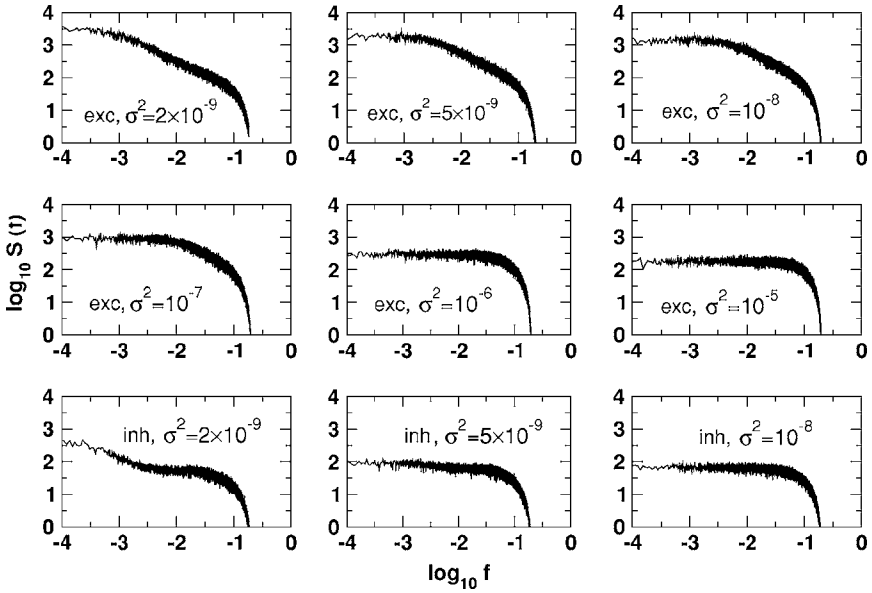

FIG. 6. Power spectra of IFR time series of excitatory (top and middle rows) and inhibitory (bottom row) units for $N=3$ and $N_E=1$. $I=0.09$.

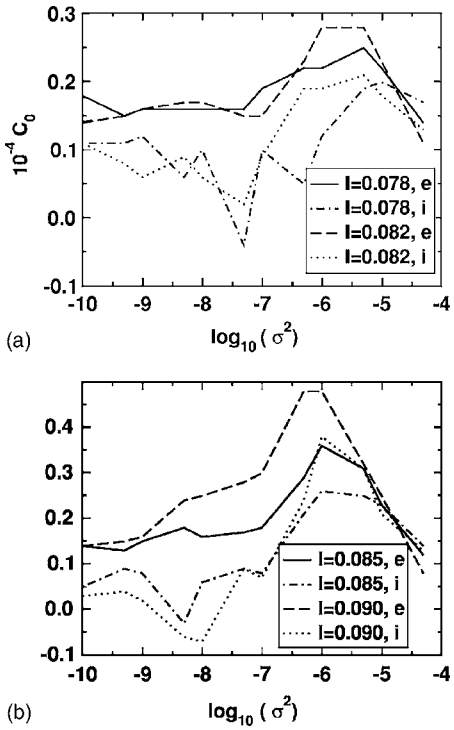

FIG. 7. Stochastic resonance-type responses in a system with $N=3$, $N_E=1$ for excitatory and inhibitory units. $S(t)=0.003\sin(2\pi t/30)$. Results are averaged over 200 trials. Total time for each trial $T=600$.

from weak to moderate values leads to an increase in the ability of excitatory units to encode the incoming signal (Fig. 7). When the noise becomes too strong, the coding ability deteriorates, giving the bell-shaped curve of C_0, characteristic of SR.

Unlike excitatory units, inhibitory ones have three possible firing regimes—a high frequency and a silent one at attractors 1 and 2, and a low-frequency one at attractor 3. Therefore, the IFR of an excitatory unit coincides with that of an inhibitory unit only for part of the time, otherwise it is zero. This results in a worse coding ability compared to that of an excitatory unit, which is shown by the lower SR-type response in Fig. 7.

A comparison of IFR with the periodic input $S(t)$ for all three units for weak, moderate, and strong noise is given in Fig. 9.

B. $N_E=0$

In this case, we set $|k|=0.1$. With this condition fulfilled, there is a double Hopf bifurcation at the same value of I as for $N_E=1$ and $|k|=0.3$. There are three limit cycles emerging at this bifurcation, which are located in invariant subspaces,

$$x_1 = x_2, \tag{6}$$

$$x_2 = x_3, \tag{7}$$

$$x_1 = x_3. \tag{8}$$

All of these cycles are 2:1 synchronized, and there are no 3:0 synchronized attractors. Moreover, they are all globally stable and no noise-driven switching is observed.

Two of these cycles are shown in Fig. 10 (left-hand and central columns). Apart from these cycles, there is a limit cycle with all units desynchronized (right-hand column), which does not belong to an invariant subspace that could be defined from the system's symmetry, and the origin of which is unclear. In the presence of noise, transitions between

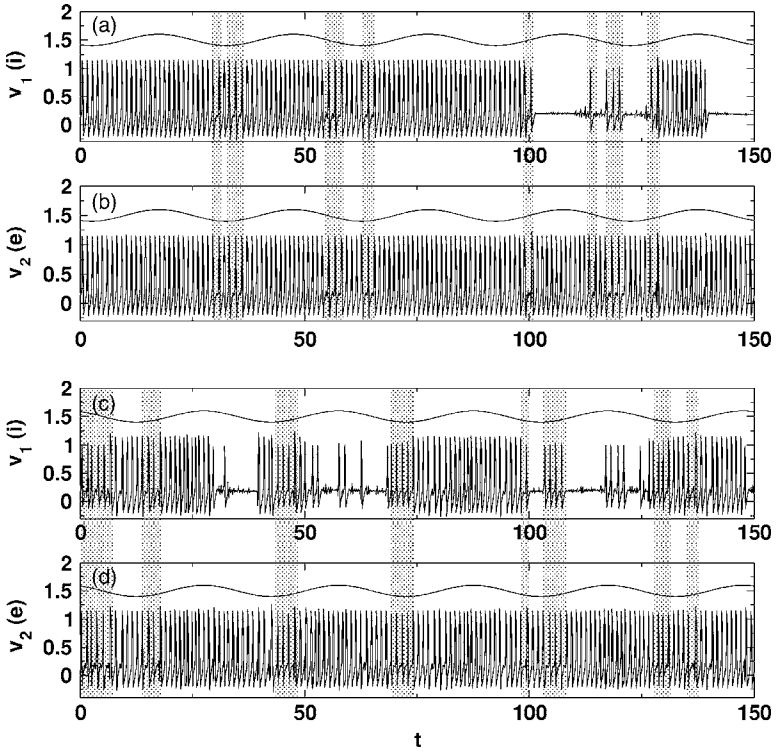

FIG. 8. Time series of excitatory and inhibitory units with a periodic input. $\sigma^2=10^{-8}$, (a) inhibitory unit, (b) excitatory; $\sigma^2=5\times10^{-7}$, (c) inhibitory unit, (d) excitatory. $N=3$, $N_E=1$, $I=0.09$, $S(t)=0.003\sin(2\pi t/30)$. Shaded areas denote visits to attractor 3. Sinusoid lines schematically represent the input.

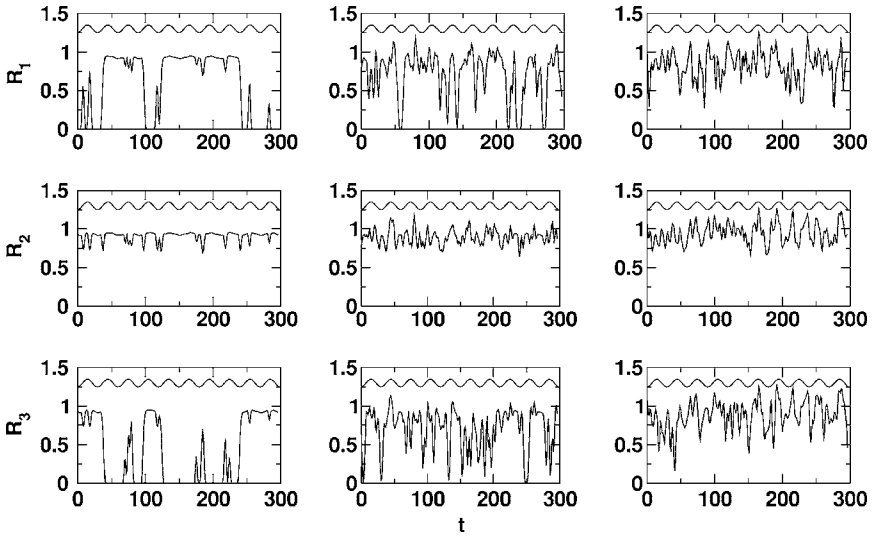

FIG. 9. Instantaneous firing rate vs periodic input for all three units with different noise intensities: $\sigma^2=10^{-8}$ (left-hand side), $\sigma^2=5\times10^{-7}$ (center), $\sigma^2=10^{-5}$ (right-hand side).

cycles do not occur. As for the case $N_E=1$, subspace (5) contains a stationary solution.

Due to the absence of itinerancy, we do not observe power-law dynamics and input-dependent selection of attractors induced by noise.

C. $N_E=2$ and $N_E=3$: Definition of balancing

In these cases there are no bifurcations for $I<I_0$, hence no stable attracting set other than the stationary state exists in that interval.

Therefore the case of $N_E=1$ has special significance. For $N_E=1$ we observe CI-like dynamics accompanied by power-law behavior with small noise and improved coding ability with increasing levels of noise, while for lower and higher N_E the system's dynamics is much simpler and does not qualitatively depend on noise. Our simulations show that this is the case for $N>3$ as well. In order for the switching to be observed, it must hold that

$$N_E = N_E^0 = [N/2] - 1. \tag{9}$$

Relation (9) gives the definition of balanced coupling, for which the system has special properties described above.

For $N_E>N_E^0$ the firing threshold of the entire system is the same as that of a single uncoupled unit (no Hopf bifurcations take place for $I\leq I_0$), while for $N_E<N_E^0$ the new threshold $I_1<I_0$ is present and multistability for $I_1<I_0$ is observed, but there are no transitions between the cycles.

It has been observed that the balancing of excitation and inhibition can bring about complex dynamics in neuronal models [29], which can be related to variability of cortical neuronal dynamics.

Simulations show that for any $N_E\leq N_E^0$ it is necessary to have

$$|k| \approx 0.1 \cdot N/(N-2N_E) \tag{10}$$

in order to keep the first Hopf bifurcation at the same parameter value (or to keep the system in the same firing range) as in the case described above for $N=3$, $N_E=1$, and $|k|=0.3$ (with $I_1\approx0.057$). Stronger coupling leads to a greater decrease in the firing threshold.

Numerically we have found that (9) and (10) are valid for at least $N\approx50$. These rules also hold for the trivial case of $N=2$, where there are no bifurcations for $N_E=1$ and 2, while for $N_E=0$ there is an ordinary Hopf bifurcation at I_1 and there is no multistability.

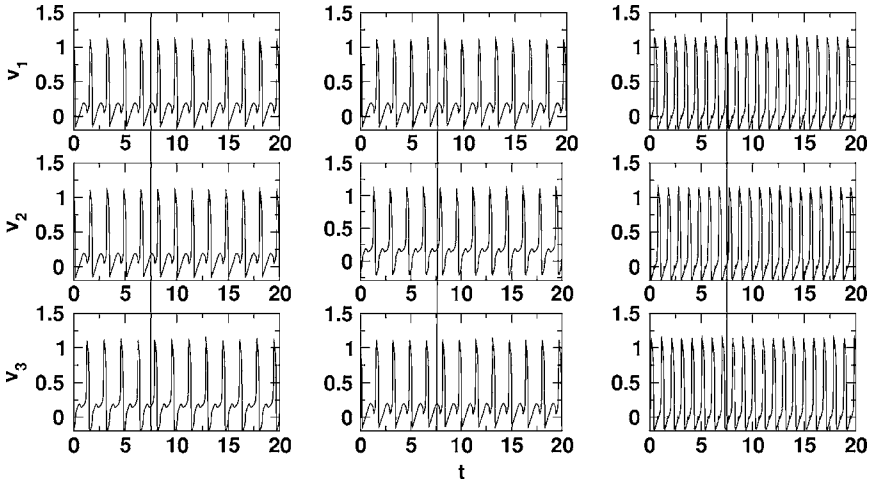

FIG. 10. Firing regimes for three different limit cycles for $N=3$, $N_E=0$, $I=0.07$, $k=0.1$. Left-hand and central columns, two units synchronized; right-hand column, all are desynchronized.

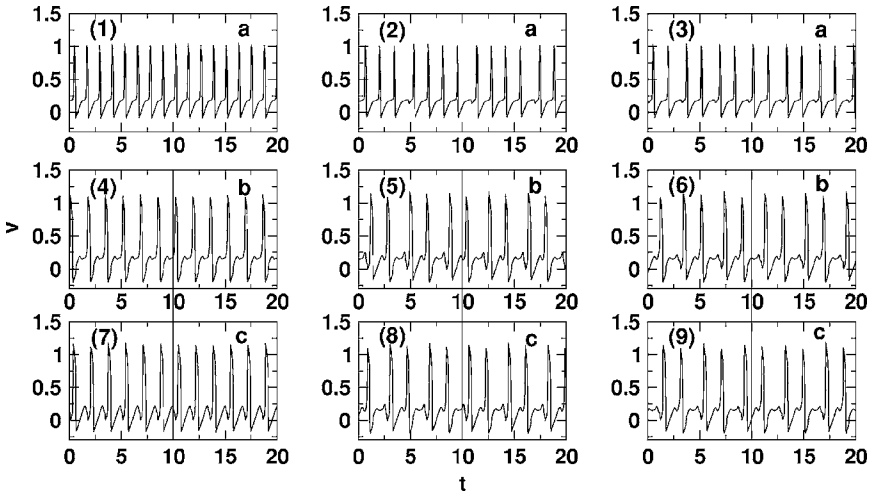

FIG. 11. Firing patterns for $N=4$, $N_E=1$, $k=0.2$. (1), (4), (7) $I=0.080$; (2) $I=0.0707$; (3) $I=0.0704$; (5), (8) $I=0.0741$; (6), (9) $I=0.0710$.

In the following section, we present a detailed study of the balanced case of $N=4$ and $N_E=1$.

III. FOUR FHN EQUATIONS WITH $N_E=1$

This case is similar to the case with $N=3$ and $N_E=1$ with some notable differences. With balancing conditions (9) and (10) satisfied, there is a triple resonant Hopf bifurcation at $I\approx 0.057$ and 11 multistable attracting sets exist for $I_1 \lesssim I \lesssim 0.090$ illustrated in Figs. 11 and 12 [each graph shows one of $v_i(t)$ plots marked by a letter]. At $I\approx 0.080$ they have the following form:

(i) a stationary solution (invariant subspace $x_1=x_2=x_3=x_4$);

(ii) a fully synchronized (4:0) limit cycle,

$$(a',a,a,a) \tag{11}$$

[subspace $x_2=x_3=x_4$, a shown in Fig. 11(1), a' in Fig. 12(1)];

(iii) three 3:1 synchronized limit cycles,

$$(b,c,b,b), \quad (b,b,c,b), \quad (b,b,b,c) \tag{12}$$

[subspaces $x_1=x_3=x_4$, $x_1=x_2=x_4$, and $x_1=x_2=x_3$; b shown in Fig. 11(4), c in Fig. 11(7)];

(iv) three 3:1 synchronized limit cycles,

$$(c,b,c,c), \quad (c,c,b,c), \quad (c,c,c,b); \tag{13}$$

(v) three 2:2 synchronized limit cycles,

$$(g,g,0,0), \quad (g,0,g,0), \quad (g,0,0,g) \tag{14}$$

[subspaces $x_1=x_2$, $x_3=x_4=C$; $x_1=x_3$, $x_2=x_4=C$; and $x_1=x_4$, $x_2=x_3=C$; g shown in Fig. 12(7)]. It is assumed that the first unit is excitatory and the other units are inhibitory.

With decreasing I these limit cycles undergo significant transformations. The behavior of the fully synchronized limit cycle (11) is similar to that of the cycle 3 for $N=3$, $N_E=1$ (Sec. III A). At certain parameter values below ≈ 0.071 the limit cycle loses stability, and there are intervals of I values, where oscillations have a larger period and are possibly aperiodic. The dependence of two Floquet multipliers with the largest absolute value of I is shown in Fig. 13. Examples of nonlimit cycle oscillations are given in Figs. 11(2) and 11(3).

The 3:1 synchronized limit cycles also demonstrate trans-

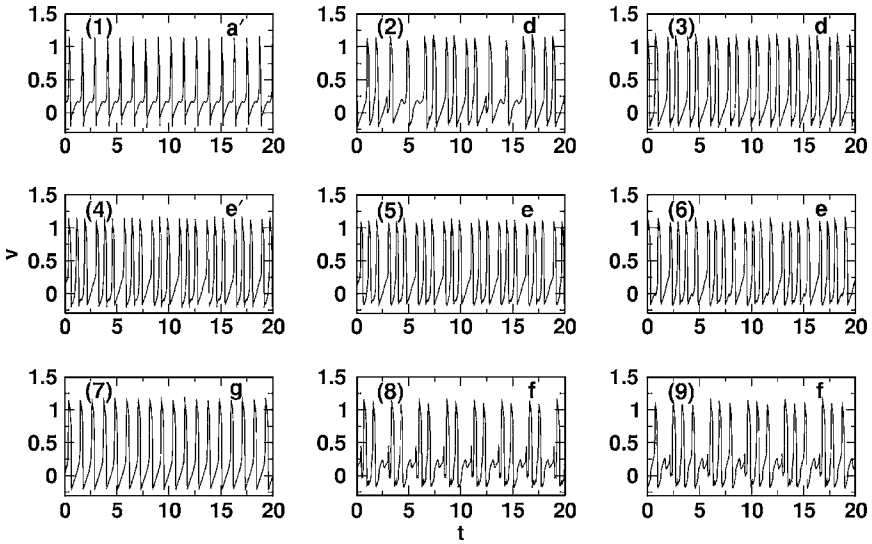

FIG. 12. Firing patterns for $N=4$, $N_E=1$, $k=0.2$. (1), (7) $I=0.080$; (2) $I=0.0741$; (3) $I=0.0710$; (4), (5), (8) $I=0.0925$; (6), (9) $I=0.0942$.

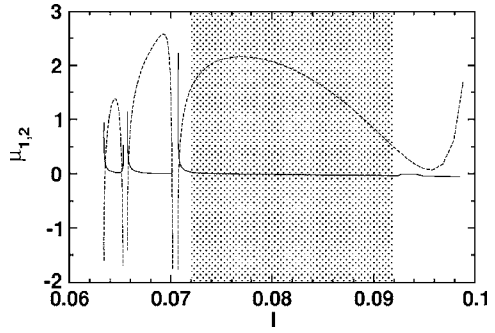

FIG. 13. Two Floquet multipliers with the largest absolute value of the attractor (11) for I values for which it is a simple limit cycle.

formations with decreasing I. At $I \approx 0.076$ they (13) bifurcate into 2:1:1 synchronized attractors

$$(d,b,d,c), \quad (d,c,b,d), \quad (d,d,c,b) \tag{15}$$

with d-units firing at a higher frequency [shown in Figs. 12(2) and 12(3)]. However, cycles (12) do not undergo such bifurcation and remain 3:1 synchronized. At lower I values, all units with b, c, and d patterns undergo bifurcations similar to those of the attractor (11) with alternating intervals of a simple limit cycle and more complex oscillations as I decreases. Examples of b, c, and d patterns for some parameter values are given in Figs. 11(5), (6), (8), and (9) and 12(2), (3), (5), and (6). The dependence of the firing rate of all patterns on the input is shown in Fig. 14.

With the increase of I, another three stable limit cycles emerge at $I \approx 0.090$.

(vi) 3:1 synchronized limit cycles,

$$(e',f,e,e), \quad (e',e,f,e), \quad (e',e,e,f) \tag{16}$$

[subspaces $x_1=x_3=x_4$, $x_1=x_2=x_4$, and $x_1=x_2=x_3$, Figs. 12(4)–(6), 12(8), and 12(9)].

As I increases further, they demonstrate complicated transformations, and the resulting firing patterns are shown in Fig. 12. These cycles also exist for $I<0.090$ and are unstable there, although they still attract trajectories in the presence of noise.

In the presence of noise for $I \lesssim 0.076$, there is itinerant dynamics between attractors (11), (12), and (15). With a periodic signal and small noise, an orbit is most likely to stay near a low-frequency attractor (12) and the probability of transition to a high-frequency attractor (11) or (15) is higher for lower input than for higher input. This results in negative correlations between the periodic input and the IFR of a single excitatory unit.

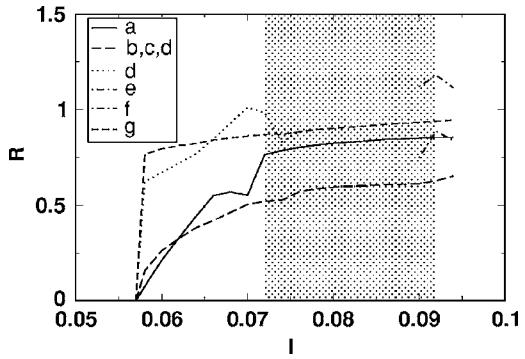

FIG. 14. Dependence of the firing rate of different firing patterns on the input I for $N=4$ and $N_E=1$. The letters correspond to Figs. 11 and 12.

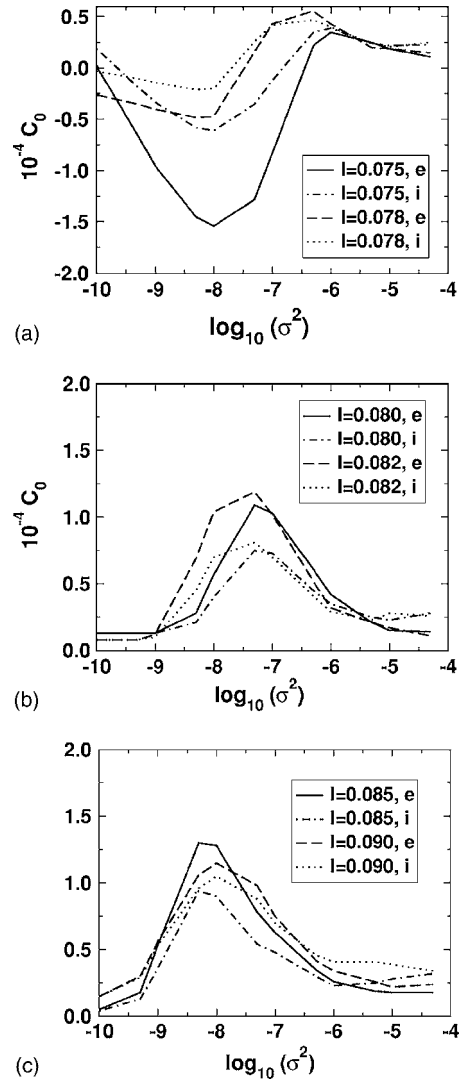

FIG. 15. Stochastic resonance-type responses in a system with $N=4$, $N_E=1$ for excitatory and inhibitory units. $S(t)=0.003\sin(2\pi t/30)$. Results are averaged over 200 trials. Total time for each trial $T=600$.

For higher I, the d-type high-frequency oscillations are not present and the intermittent dynamics takes place between (11)–(13) and (16). The probability of choosing a high-frequency attractor is higher at a maximal input, therefore the $C_0(\sigma^2)$ dependence becomes similar to that of the case of $N=3$, $N_E=1$ [Figs. 15(b) and 15(c)]. With $I \gtrsim 0.09$ no SR-like dynamics is observed.

For all I values, limit cycles (14) are never visited. Since firing patterns of excitatory and inhibitory units do not have significant differences, their spectral properties are also similar, unlike in the $N=3$, $N_E=1$ case.

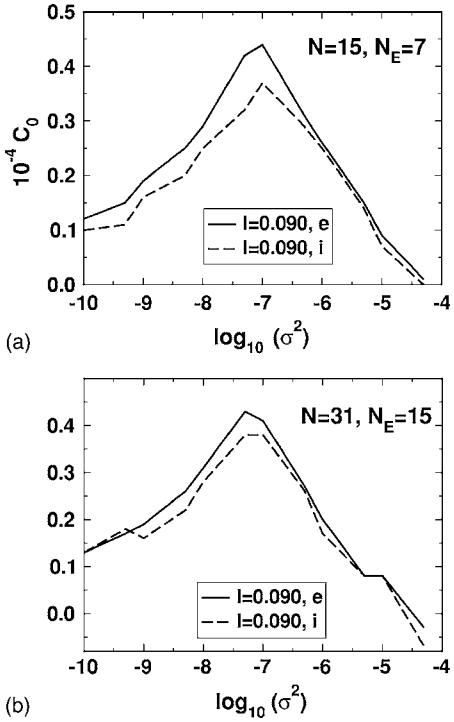

FIG. 16. Stochastic resonance-type responses in a system with $N=15$ and $N=31$ for excitatory and inhibitory units. $S(t)=0.003\sin(2\pi t/30)$. Results are averaged over 200 trials. Total time for each trial $T=600$.

IV. HIGHER DIMENSIONS

From examining the cases of N up to about 50, we can conclude that higher-dimensional cases can be reduced to those of $N=3$ and $N=4$, provided balancing conditions (9) and (10) hold.

For all N, there is a multiple Hopf bifurcation at I_1 with $N-1$ pairs of equal eigenvalues crossing the imaginary axis, producing a number of limit cycles.

For odd N, there are many different limit cycles, but transitions take place only between N_E of $N:0$ synchronized cycles (analog of cycle 3) and $N-N_E$ of $(N-1):1$ synchronized cycles with one silent unit (analogs of cycles 1 and 2). The dynamics of an excitatory unit is not different from that for $N=3$ (it also iterates between high- and low-frequency oscillations). For an inhibitory unit, since a shorter time is spent in the silent regime with growing N (because there are $N-N_E$ cycles with only one unit silent), the dynamics becomes similar to that of an excitatory unit. SR-like properties of systems with higher odd dimensions are also similar to those of systems with $N=3$. Figure 16 shows the $C_0(\sigma^2)$ dependence for $N=15$ and $N=31$ with the same input.

For even N the dynamics is more complicated, but similar in general to the $N=4$ case. It should be noted that for higher dimensions, the findings described (multistability, CI-like dynamics and adaptability to the input) are observed only if the balancing condition (9) is satisfied. Changing the number of excitatory units by just one results in a dramatic change in the dynamics, i.e., for higher N the case of $N_E=N_E^0-1$ is equivalent to the case of $N_E=0$ for $N=3$, and the case of $N_E=N_E^0+1$ is equivalent to the case of $N_E=2$ for $N=3$.

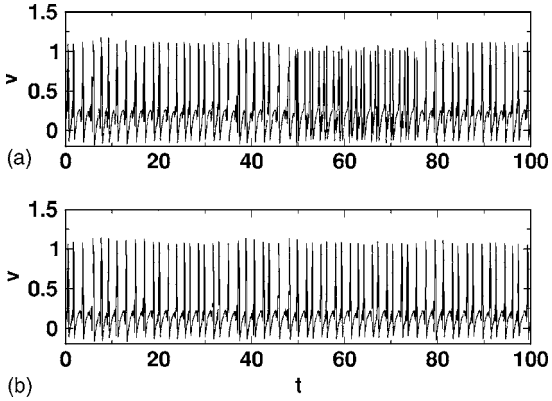

FIG. 17. Firing patterns of inhibitory (a) and excitatory (b) units of system (17). $I=0.075$. The inhibitory unit oscillates between slower and faster firing regimes.

This is related to the mode of coupling in Eq. (1). For each equation the coupling term is equivalent to the same sum of excitatory and inhibitory influences regardless of the system size, and the removal or addition of a single unit results in the same changes for any N.

The strict balancing condition (9) can be weakened by introducing a different mode of coupling such that a minor change of excitatory and/or inhibitory units does not significantly affect the balanced system's encoding ability. For example, we consider a synapse-type coupling mode adopted from Ref. [30],

$$\varepsilon\dot{v}_i = v_i(v_i-a)(1-v_i) - w_i + I + S(t) + \frac{1}{N}\sum_{j=1}^{N} k_{ij}G(v_j) + \xi_i(t),$$

$$\dot{w}_i = v_i - w_i - b, \tag{17}$$

where G is a sigmoidal function $G(x)=1/(1+\exp\{[-(x-\theta)]/\alpha\})$ with the threshold θ and the width α. We present here a test case of $N=26$ with $\theta=0.5$, $\alpha=0.3$, and all $k_{ij}=0.04$.

For $N_E\leqslant 13$ there is no firing for subthreshold input, while for $N_E\geqslant 17$ there is a single firing regime with the firing rate insignificantly changing with I. In contrast, for $14\leqslant N_E\leqslant 16$ there is a multistability of at least two firing regimes with noise-induced transitions between them. Figure 17 shows typical spike trains from units of both types for $N_E=14$. While multistability and itinerant behavior are observed for all three values of N_E, the coding ability deteriorates with the increasing number of excitatory units [Fig. 18(a)]. However, the deterioration is not as abrupt as that for the system (1) [Fig. 18(b)].

Whether different equations other than FHN with dynamical coupling would lead to a looser balancing condition requires further research; such generalizability may be important if this model is to be used as an architectural, not a functional, model of the brain.

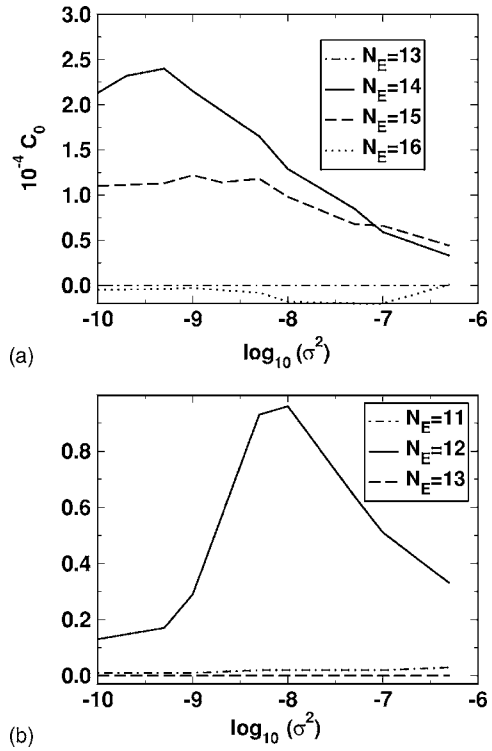

FIG. 18. Stochastic resonance-type responses in system (17) for excitatory and inhibitory units. The results are averaged over 200 trials. Total time for each trial $T=600$. (a) System (17) with $N=26$ and $I=0.075+0.005\sin(2\pi t/30)$. (b) System (1) with $N=26$ and $I=0.080+0.003\sin(2\pi t/30)$.

V. DISCUSSION

Collections of nonlinear oscillators encountered in biological organisms are frequently quite adaptable to changes in the external environment. The brain, for instance, is a highly adaptable organ in spite of the limited *short time* plasticity embedded in single oscillators and/or their connection strengths. Indeed, recent studies have shown that brain-wide, frequency-specific neural synchrony and asynchrony, or the dynamical attractor selection among multiple neural oscillators, seem to be involved in the generation of perceptual, cognitive and behavioral processes in response to external and/or internal stimuli [31]. In the present study, we have examined a simple model of this sort of emergent adaptability by using small dimensional coupled FHN oscillators.

The key finding here is that, when the numbers of excitatory or inhibitory oscillators are in a specific relation, or the system has balanced coupling, the addition of intermediate noise considerably increases covariance between input external forcing and the mean oscillatory rate or the activity levels over the whole network, just like what is known as the SR phenomenon [8,10]. This noise-induced adaptive response in coupled oscillators is associated with noise-driven switching among multistable limit cycles, of which the dynamics have a long-range time correlation.

We have studied the detailed dynamical structures of these multistable limit cycles in the presence of noise to explain why the selection of multistable attractors with different activity levels is statistically more ordered in response to the changes in the external forcing. It has been found that the chance of a revisit to a subspace containing low-frequency limit cycles is higher for lower external forcing. Thus, we have found a phenomenon leading to network adaptability due to the statistically ordered selection and/or deselection of multistable attractors with different intrinsic frequencies.

The beneficial role of noise in biological systems has indeed been extensively studied over the past decade, especially for the phenomenon of SR [8,10], which is generally defined as the optimization of responses of a nonlinear system to a weak input signal caused by external noise. For instance, in neural systems SR has been shown to optimize sensitivity of sensory neurons [32], which may lead further to the enhancement of perception and/or behavior in animals [33] and humans [34].

As a natural extension to these studies, it has recently been demonstrated that externally added noise can enhance input-output coherence within the human brain [35–38]. The improved responses were observed at the level of the brain stem neuronal networks, where the neurological noise can help trigger changes in heart rate in response to small changes in blood pressure [35,38], as well as at the level of the cortices, including the visual areas, where visual noise can enhance responses in the brain waves [36] and behavioral output [37] to weak visual signals. These results indicate that the brain can also work as a stochastic resonator.

However, unlike dynamical systems such as overdamped bistable systems or monostable systems with a response threshold—the latter being used as a model of a sensory neuron—for which the theory of SR has been rigorously studied [10], neuronal networks within the brain may not have a definite threshold or bistability. Rather, the brain can be regarded as mutually coupled excitable and/or oscillatory units [31] capable of showing multistable dynamics, with only a limited number of distributed local networks of neurons interacting together involved in cortical information processing [15,31] and brain stem neuronal dynamics [39], but including both excitatory and inhibitory connections [15,39].

Our model is in fact equipped with many such global dynamical signatures of the brain at work, namely mutual interaction between local neural assemblies [31], the existence of ongoing dynamics, which is often long-range correlated [40], the emergence of transient synchronization and desynchronization [31,41,42], and SR-like behavior [35–38]. As such, it is highly relevant for the study of the global dynamics of the brain under the influence of both internal and external noise.

ACKNOWLEDGMENTS

The authors thank D. Nozaki, T. Nomura, and A. Takamatsu for discussion. This study was supported by the Japan Science and Technology Agency (Y.Y.) and the Japan Society for the Promotion of Science (L.A.S.).

[1] A. T. Winfree, *The Geometry of Biological Time* (Springer, Berlin, 1980).
[2] L. Glass, Nature (London) **410**, 277 (2001).
[3] R. FitzHugh, Biophys. J. **1**, 445 (1961); J. Nagumo, S. Arimoto, and S. Yoshizawa, Proc. IRE **50**, 2061 (1960).
[4] A. L. Hodgkin and A. F. Huxley, J. Physiol. (London) **117**, 500 (1952).
[5] Y. Kuramoto, *Chemical Oscillations, Waves, and Turbulence* (Springer, Berlin, 1984).
[6] K. Ikeda, K. Matsumoto, and K. Otsuka, Prog. Theor. Phys. Suppl. **99**, 295 (1989); K. Kaneko, Physica D **41**, 137 (1990); K. Kaneko and I. Tsuda, Chaos **13**, 926 (2003).
[7] A. Takamatsu, R. Tanaka, and T. Fujii, Phys. Rev. Lett. **92**, 228102 (2004); A. Takamatsu, R. Tanaka, H. Yamada, T. Nakagaki, T. Fujii, and I. Endo, *ibid.* **87**, 078102 (2001); A. Takamatsu, T. Fujii, and I. Endo, *ibid.* **85**, 2026 (2000).
[8] K. Wiesenfeld and F. Moss, Nature (London) **373**, 33 (1995).
[9] B. Lindner and L. Schimansky-Geier, Phys. Rev. E **60**, 7270 (1999); S. G. Lee, A. Neiman, and S. Kim, *ibid.* **57**, 3292 (1998).
[10] L. Gammaitoni, P. Hänggi, P. Jung, and F. Marchesoni, Rev. Mod. Phys. **70**, 223 (1998).
[11] R. L. Honeycutt, Phys. Rev. A **45**, 600 (1992).
[12] The Floquet multipliers are calculated using XPPAUT 5.85 (http://www.math.pitt.edu/~bard/xpp/xpp.html).
[13] S. A. Campbell and M. Waite, Nonlinear Anal. Theory, Methods Appl. **47**, 1093 (2001).
[14] P.-L. Gong and J.-X. Xu, Phys. Rev. E **63**, 031906 (2001).
[15] M. Rabinovich, R. Huerta, M. Bazhenov, A. K. Kozlov, and H. D. I. Abarbanel, Phys. Rev. E **58**, 6418 (1998).
[16] W. J. Freeman, Chaos **13**, 1067 (2003).
[17] L. M. Kay, Chaos **13**, 1057 (2003).
[18] A. Raffone and C. van Leeuven, Chaos **13**, 933 (2003).
[19] S. K. Han and D. E. Postnov, Chaos **13**, 1105 (2003).
[20] S. Nara, Chaos **13**, 1110 (2003).
[21] H. Kitajima, T. Yoshinaga, K. Aihara, and H. Kawakami, Chaos **13**, 1122 (2003).
[22] H. Fujii and I. Tsuda, Neurocomputing **58–60**, 151 (2004).
[23] V. S. Afraimovich, V. P. Zhigulin, and M. I. Rabinovich, Chaos **14**, 1123 (2004); A. Venaille, P. Varona, and M. I. Rabinovich, Phys. Rev. E **71**, 061909 (2005).
[24] F. T. Arecchi, R. Meucci, G. Puccioni, and J. Tredicce, Phys. Rev. Lett. **49**, 1217 (1982); F. T. Arecchi, Chaos **1**, 357 (1991).
[25] S. Kraut, U. Feudel, and C. Grebogi, Phys. Rev. E **59**, 5253 (1999).
[26] C. Masoller, Physica D **168**, 171 (2002).
[27] Hanning window filtered IFR is defined as follows. If t_i are firing times, then the spike train is $s(t)=\Sigma\delta(t-t_i)$, and the IFR is $r(t)=\int_{-T/2}^{T/2}\cos[4\pi(t-\tau)/T]s(\tau)d\tau$, where T is the window width, $T=10$.
[28] N. G. Stocks, Phys. Rev. E **63**, 041114 (2001); D. Rousseau, F. Duan, and F. Chapeau-Blondeau, *ibid.* **68**, 031107 (2003).
[29] C. van Vreeswijk and H. Sompolinsky, Science **274**, 1724 (1996); Neural Comput. **10**, 1321 (1998).
[30] H. Hasegawa, Phys. Rev. E **67**, 041903 (2003).
[31] F. Varela, J.-P. Lachaux, E. Rodriguez, and J. Martinerie, Nat. Rev. Neurosci. **2**, 229 (2001).
[32] J. K. Douglas, L. Wilkens, E. Pantazelou, and F. Moss, Nature (London) **365**, 337 (1993); J. E. Levin and J. P. Miller, *ibid.* **380**, 165 (1996); J. J. Collins, T. T. Imhoff, and P. Grigg, J. Neurophysiol. **76**, 642 (1996); D. Nozaki, D. J. Mar, P. Grigg, and J. J. Collins, Phys. Rev. Lett. **82**, 2402 (1999).
[33] D. F. Russell, L. A. Wilkens, and F. Moss, Nature (London) **402**, 291 (1999).
[34] J. J. Collins, T. T. Imhoff, and P. Grigg, Nature (London) **383**, 770 (1996); K. A. Richardson, T. T. Imhoff, P. Grigg, and J. J. Collins, Chaos **8**, 599 (1998); E. Simonotto, M. Riani, C. Seife, M. Roberts, J. Twitty, and F. Moss, Phys. Rev. Lett. **78**, 1186 (1997).
[35] I. Hidaka, D. Nozaki, and Y. Yamamoto, Phys. Rev. Lett. **85**, 3740 (2000).
[36] T. Mori and S. Kai, Phys. Rev. Lett. **88**, 218101 (2002).
[37] K. Kitajo, D. Nozaki, L. M. Ward, and Y. Yamamoto, Phys. Rev. Lett. **90**, 218103 (2003).
[38] R. Soma, D. Nozaki, S. Kwak, and Y. Yamamoto, Phys. Rev. Lett. **91**, 078101 (2003).
[39] S. M. Barman and G. L. Gebber, J. Neurophysiol. **57**, 1410 (1987); **61**, 1011 (1989); S. M. Barman, H. S. Orer, and G. L. Gebber, *ibid.* **74**, 2295 (1995).
[40] M. Yamamoto *et al.*, Brain Res. **366**, 279 (1986); M. C. Teich, IEEE Trans. Biomed. Eng. **BME-36**, 150 (1989); C. D. Lewis *et al.*, J. Neurophysiol. **85**, 1614 (2001).
[41] P. A. Tass, T. Fieseler, J. Dammers, K. Dolan, P. Morosan, M. Majtanik, F. Boers, A. Muren, K. Zilles, and G. R. Fink, Phys. Rev. Lett. **90**, 088101 (2003).
[42] J. M. Hurtado, L. L. Rubchinsky, and K. A. Sigvart, J. Neurophysiol. **91**, 1883 (2003); A. A. Kuhn, D. Williams, A. Kupsch, P. Limusin, M. Hariz, G. H. Schneider, K. Yarrow, and P. Brown, Brain **127**, 735 (2004).